Cellulose (2020) 27:5241–5253
https://doi.org/10.1007/s10570-020-03139-0

ORIGINAL RESEARCH

Multiscale cellulose based self-assembly of hierarchical structure for photocatalytic degradation of organic pollutant

Lingfeng Yan · Baojiang Liu · Weiya Li · Tao Zhao · Yatao Wang · Qiangqiang Zhao

Received: 13 January 2020 / Accepted: 1 April 2020 / Published online: 11 April 2020

Abstract The treatment of wastewater generated by textile industry has attracted researchers' attentions, and photocatalysis is considered as a good strategy to solve this problem because of the strong redox capacity. Herein, a novel visible light-responsive cotton-PPy-MWCNTs-$BiVO_4$ photocatalytic material with the hierarchical structure was successfully prepared by a simple layer assembly method. The composite material has excellent degradation performance for reactive brilliant blue (RB-19) dye solution, and the degradation efficiency can reach 97.8% under visible light irradiation for 2 h. The performance improvement is mainly ascribed to the interaction between polypyrrole (PPy) and multi-walled carbon nanotubes (MWCNTs) in the system, where PPy can efficiently transfer holes and MWCNTs can separate electrons, thereby greatly speeding up the separation of photogenerated carriers. The loading of $BiVO_4$, PPy and MWCNTs on cotton fabrics exhibits better stability and recyclability than traditional powdery photocatalysts. In sum, this paper provides a feasible idea for the application of flexible cellulose-based photocatalytic materials.

Keywords $BiVO_4$ · Self-assembly · Photocatalytic cotton fabric · Ppy · Mwcnts

L. Yan · B. Liu · T. Zhao · Q. Zhao (✉)
Key Laboratory of Textile Science & Technology, Ministry of Education, College of Chemistry, Chemical Engineering and Boitechnology, DongHua University, Shanghai 201620, China
e-mail: qqzhao@dhu.edu.cn

B. Liu · Y. Wang
Coal Chemical R&D Center of Kailuan Group, Hebei Provincial Technology Innovation Centre of Coal-Based Materials and Chemicals, Tangshan 063018, Hebei Province, China

W. Li
3trees Paint Co. Ltd., Putian 351100, Fujian, China

Introduction

With the development of industrialization, environmental pollution and energy shortages have increasingly received attention (Trowbridge et al. 2018). Photocatalysis has been considered as one of the best strategies to solve these problems because it shows great potential in the field of photocatalytic hydrogen evolution (Ran et al. 2017; Wang et al. 2019; Zhang et al. 2016), CO_2 photoreduction (Crake et al. 2019; Dai et al. 2017; Tasbihi et al. 2018) and photocatalytic degradation of pollutants (Dong et al. 2019; Li et al. 2019; Xu et al. 2019). For the treatment of pollutants, compared with the traditional strategies, such as physical adsorption (Kyzas and Matis 2015; Ma et al. 2014) and chemical oxidation (Wacławek et al. 2017), photocatalysis has the competitive advantages of low secondary pollution and operating cost. Therefore, the mechanism and application have been the

important research parts in the photocatalysis field (A et al. 2018; Komeily-Nia et al. 2019). With the deepening of research, a fairly reliable mechanism has been proposed (Xiao et al. 2018). The semiconductor photocatalyst absorbs light when the energy of the photo is equal to or larger than the band gap of semiconductor, and the electrons on the valence band (VB) is subsequently excited onto the conduction band (CB). Thus, photogenerated electrons can be generated on the CB and holes can be formed on the VB. The photogenerated electrons and holes will be adopted in reduction and oxidation reaction. Generally, the photocatalytic reaction consists of three main steps: (1) Photoexcitation generates electrons and holes; (2) Electrons are separated from holes and transferred to the surface; (3) Reduction and oxidation reaction occurs on the surface. However, during the second step, only about 5% (Legrini et al. 1993) of the electrons and holes are involved in the catalytic process, and most of the electrons and holes (about 95%) recombine. For this reason, the research on improving the photocatalyst stability and the charge carrier separation efficiency is a main issue in photocatalysis.

$BiVO_4$ is a suitable photocatalytic material to solve the above problems thanks to its favorable stability, suitable band gap and low cost (Yang et al. 2020). $BiVO_4$ mainly has three crystal forms, including orthorhombic pucherite, tetragonal dreyerite, and monoclinic clinobisvanite. The monoclinic $BiVO_4$, which possesses a band gap of 2.4 eV, shows better photocatalytic activity than other types of $BiVO_4$ in the visible region (Safaei et al. 2018). However, the photocatalytic efficiency of monoclinic $BiVO_4$ is also limited due to the high electron–hole recombination and short hole diffusion length. Therefore, numerous methods are used to strengthen its performance. For example, the enhancement can be obtained by forming the heterojunction with other catalysts (Liu et al. 2019; Lv et al. 2015; Wang et al. 2018). Heterojunction can significantly improve the charge separation efficiency and broaden the light absorption range, which enhances the photocatalystic performance accordingly. In addition, the introduction of conductive materials like graphene oxide (GO) and Ag is also a good strategy to overcome the mentioned challenges (Yang et al. 2019). Ning Lv et al. constructed a series of $GO/TiO_2/Bi_2WO_6$ composite photocatalysts by solvothermal method and found that the introduction of GO reduced the crystal size of the composite catalyst and greatly enhanced the separation efficiency of the charge (Lv et al. 2019). Besides, Z-scheme WO_3/Ag/Bi_2WO_6 had been constructed by the ordinary composite method and exhibited excellent degradation effect. The better degradation effect was benefited from the Z-scheme structure and Ag NPs, which reduced the recombination of photogenerated charge and increased light absorption range (Zhou et al. 2019).

Similarly, when a suitable conductive material is added to the $BiVO_4$, the problem of high charge recombination rate can be improved, and photocatalytic performance can be enhanced. Multi-walled carbon nanotubes (MWCNTs) have been widely used in the fields of medicine, architecture and energy due to its extremely high conductivity and good mechanical property (Wu et al. 2017b). Therefore, MWCNTs as conductors of photogenerated electrons have received increasing attention in the field of photocatalysis. In the preliminary work of the Task Force, a composite photocatalytic material based on $BiVO_4$, MWCNTs and Bi_2WO_6 was successfully prepared and exhibited the good catalytic performance on the soil treatment (Lin et al. 2016). Besides, Zhao et al. synthesized $BiVO_4$ @ MWCNTs photocatalytic composite by one-step hydrothermal method. MWCNTs were successfully embedded in $BiVO_4$, and the good degradation effect on rhodamine B were obtained (Zhao et al. 2017). Thence, MWCNTs are chosen as a conductive material in this work to be compounded with $BiVO_4$.

Polypyrrole (PPy), which is considered as an excellent conductive material due to its π-conjugated heterocyclic structure, easy synthesis method and ideal stability, has also received great attention in the field of photocatalysis. Han et al. demonstrated the introduction of PPy on g-C_3N_4 by in-situ polymerization and proposed a new understanding of the role of PPy in composite catalysts. It was found that PPy not only transferred photogenerated electrons but also acted on holes (Han et al. 2018). Similarly, Liu et al. designed a system of BiOBr-Ag-PPy and verified its highly efficient catalytic ability. The underlying mechanism was PPy acted as a good hole acceptor to accelerate charge separation, thereby enhancing catalytic degradation (Liu and Cai 2018). The above works show that PPy, as a receiver and transmitter of holes, can greatly enhance separation efficiency of

photogenerated electrons and holes. Hence, we designed a ternary system containing $BiVO_4$, MWCNTs and PPy to improve the carrier separation efficiency and $BiVO_4$ catalytic activity by taking advantage of MWCNTs' ability to transmit electrons and using PPy as a hole receptor.

Except for the charge separation, another challenge in designing an efficient photocatalyst is to improve the recyclability. The conventional powder photocatalysts are not the good candidates because of its recyclability and safety. To overcome these shortcomings, the most useful method is to fix the catalyst on a reusable substrate (Komeily-Nia et al. 2019). Among them, cotton fabric is a good choice due to its good biocompatibility, environmental friendliness and accessibility (Fan et al. 2019). In this paper, the PPy-MWCNTs-$BiVO_4$ ternary system was loaded on the cotton fabrics by simple layer assembly. Specifically, in-situ polymerization was used to spread PPy evenly on the surface of cotton fabric. MWCNTs were attached to PPy driven by the electrostatic force and $BiVO_4$ was finally introduced and adhered to the composite surface by intermolecular forces between the surfaces. Subsequently, RB-19 was used as an indicator to verify the photocatalytic performance and cycle stability of the composite system. The composition and properties of the catalyst were clarified by SEM, XPS and other characterizations. Finally, a proposed mechanism was investigated by the free radical trapping experiments.

Experiment

Materials and reagents

Pyrrole monomer (Py) was obtained from Aladdin Reagents Co., Ltd. Barium nitrate pentahydrate ($BiNO_3{\cdot}5H_2O$), ammonium metavanadate (NH_4VO_3), sodium hydroxide (NaOH), nitric acid (HNO_3), ferric chloride hexahydrate ($FeCl_3{\cdot}6H_2O$), sodium dodecylbenzene sulfonate (SDBS), sodium hypophosphite (NaH_2PO_2) were purchased from Sinopharm Chemical Reagent Co., Ltd. Carbon nanotube (MWCNTs, Purity $>$ 95%, -COOH content: 3.86 wt%) was provided by XFMANO, INC. Cotton fabric (120 g/m^2) was obtained from Sequel Group, China. Reactive brilliant blue (RB-19) was purchased from Dystar Printing and Dyeing Technology Co., Ltd. Sodium oxalate (Na-OA, purity 99%), 2-methyl-2-propanol (t-BuOH, purity 99%) and 1,4-p-benzoquinone (BQ, purity 99%) were all provided by Adamas Reagent Co., Ltd. All the chemicals were used without further purification except for specific mention.

Preparation of $BiVO_4$

$BiVO_4$ was prepared through the previously reported protocol (Wang et al. 2020). 1.94 g of $Bi(NO_3){\cdot}5H_2O$ was dissolved in 5 mL of 4 mol/L of nitric acid, then 25 mL of deionized water was added to form solution A. 0.468 g of NH_4VO_3 were dissolved in 20 mL of 1 mol/L of NaOH, and mixed with 10 mL of deionized water to fabricate solution B. Finally, solution B was added dropwise to A under magnetic stirring, and the pH of the mixed solution was adjusted to 3 by adding NaOH solution. The prepared solution was transferred into a Teflon-lined autoclave and maintained at 180 °C for 4 h. The obtained product was treated with suction filtration and washed with deionized water/ethanol to remove the impurities before drying at 60 °C.

Preparation of cotton-PPy composite fabric

Pyrrole monomer was deposited on the surface of cotton fabric by in-situ polymerization. Firstly, 0.16 mL of pyrrole was added into 200 mL of deionized water and well dispersed under ultrasonic conditions for 10 min. 3 g of treated cotton fabric (washed by 50 mL 50% ethanol solution with ultrasound sonication for 60 min) was added to the pyrrole solution. At the same time, 0.13 g of $FeCl_3{\cdot}5H_2O$ (the mole ratio of pyrrole to oxidant is 1:2) was dissolved in 20 mL of deionized water and added dropwise to the cotton/pyrrole mixed solution. The final solution was incubated for three hours under magnetic agitation. The cotton was recovered when the color changed from white to off-white, and washed thoroughly prior to drying at 60 °C to obtain cotton-PPy composite fabric.

Preparation of cotton-PPy-MWCNTs composite fabric

100 mg of MWCNTs and 100 mg of SDBS were added into 100 mL of deionized water and dispersed under ultrasonication for 30 min, followed by

introducing 0.2 g of sodium hypophosphite and ultrasonicating for 10 min to obtain an ink-like solution. Subsequently, cotton-PPy composite fabric prepared in the previous step was immersed in the solution and the mixture was ultrasonicated for 15 min. Finally, the fabric was washed with deionized water and dried at 60 °C to obtain cotton-PPy-MWCNTs composite fabric.

Preparation of cotton-PPy-MWCNTs-$BiVO_4$ composite fabric

0.1 g of $BiVO_4$ and 0.01 g of PEG2000 were added into 50 mL of deionized water and ultrasonicated for 30 min to obtain a uniform suspension. Then the cotton-PPy-MWCNTs composite fabric was immersed into the suspension and the mixture was slowly stirred in an 80 °C water bath for 2 h. The composite fabric was recovered with a black surface covered by a yellow layer. Cotton-PPy-MWCNTs-$BiVO_4$ composite was obtained after washing with deionized water and drying at 60 °C. The preparation scheme of cotton-PPy-MWCNTs-$BiVO_4$ fabrication is shown in Fig. 1.

Characterization

Field emission scanning electron microscopy (FE-SEM, Hitachi SU8220, Japan) was used to observe the surface topography of the prepared sample. X-ray photoelectron spectroscopy (XPS, Escalab 250Xi, Thermo Fisher) was employed to study the chemical composition of photocatalysts. The crystal structure of the catalyst was measured by X-ray diffraction (XRD, Bruker D8 ADVANCE). The light absorption properties of the catalyst were obtained by UV–Vis diffuse reflection spectra (DRS, Lambda 900) in the wavelength range between 200–800 nm. Separation efficiency of charges were characterized by PL spectra on a PTI QM/TM fluorescence spectrometer with the excitation at 325 nm. Electrochemical impedance spectroscopy (EIS) and photocurrent response density were measured by electrochemical analyzer (model PGSTAT302N).

Degradation experiment

Dye degradation experiments were used to evaluate the photocatalytic performance of the catalyst. The experiment was carried out in a 70 mL quartz tube, in which unloaded cotton and fitted cotton fabric after loading (3×3 cm^2) floated in RB-19 solution (50 mL, 70 mg/L). The reaction system was held at a constant temperature environment (about 15 °C) and the Xe lamp (1000 w) was used as the light source. 7 mL of solution was continuously taken out every 30 min and centrifuged. The concentration of RB-19 was tested by visible spectrophotometer (HitachiU3310).

Results and discussion

Catalyst characterization

The surface morphology of cotton fabrics and composite photocatalytic cotton fabric are obtained by SEM, as shown in Fig. 2. The untreated cotton fabric surface is very smooth (Fig. 2a, b). However, as the introduction of PPy, the film-like substance is attached

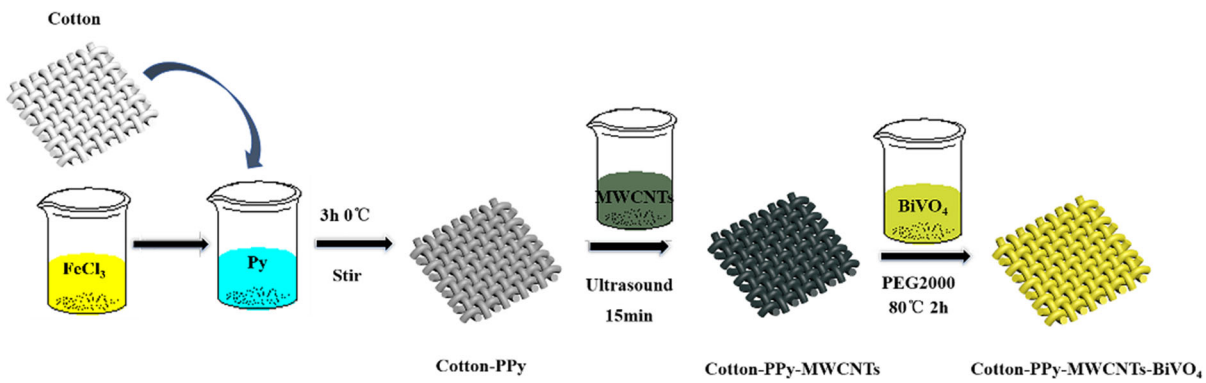

Fig. 1 Preparation of Cotton-PPy-MWCNTs-$BiVO_4$ composite cotton fabric

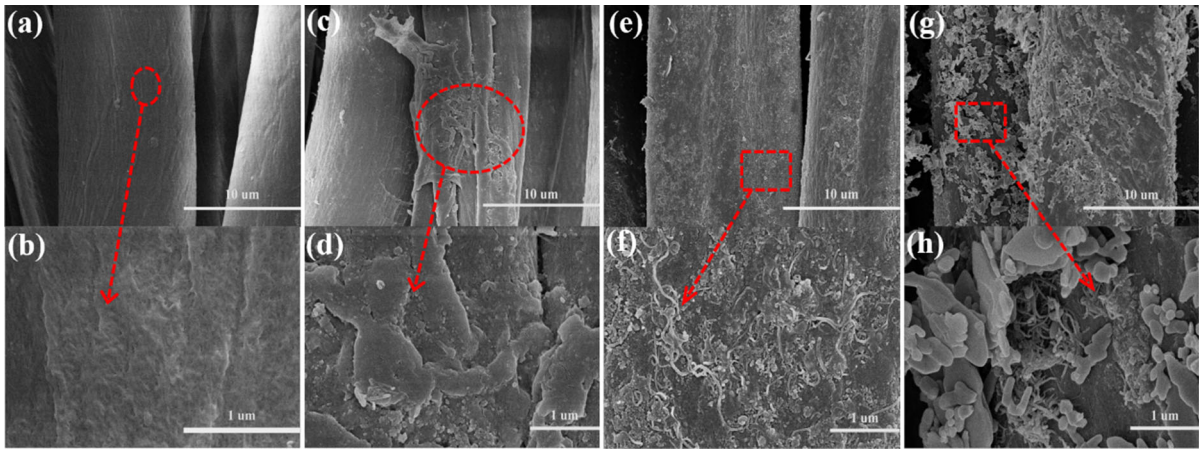

Fig. 2 the FE-SEM of composite cotton fabrics; **a**, **b** cotton; **c**, **d** cotton-PPy; **e**, **f** cotton-PPy-MWCNTs; **g**, **h** cotton-PPy-MWCNTs-$BiVO_4$

to the surface of the cotton fabric in Fig. 2c, d. Numerous PPy particles are founded on the cotton surface, which confirms the successful loading of PPy. The SEM images of cotton-PPy-MWCNTs three-component composite fabric are presented in Fig. 2e, f. The tubular structures and granular structures can be clearly observed, indicating the good compatibility and tight integration between MWCNT and PPy. The images of cotton-PPy-MWCNTs-$BiVO_4$ in Fig. 2g, h show that the $BiVO_4$ flakes are attached to the substrate. A close connection among $BiVO_4$, PPy and MWCNTs also can be observed, which is helpful for the charge separation. Obviously, the results of SEM prove the successful establishment of cotton-PPy-MWCNTs-$BiVO_4$ four-component system and the tight connection between each component.

The element composition and distribution of the composite cotton fabric are tested by EDS. As shown in Fig. 3, there are (C, N, O, Bi and V) five elements on the surface of composite cotton fabric. The large amount of C, N and O element are assigned to carbon-containing functional groups in cotton fibers, PPy and MWCNTs, and the presence of Bi and V is attributed to flakes of $BiVO_4$. The above EDS analyzes confirm that PPy, MWCNTs and $BiVO_4$ were successfully loaded on cotton fabric surface.

X-ray diffraction (XRD) is used to study the crystal structure and phase composition of the catalyst. As shown in Fig. 4, all diffraction peaks of cotton-PPy-MWCNTs-$BiVO_4$ can be corresponded to monoclinic of $BiVO_4$ (ICDD PDF#75–1867). Notably, the characteristic diffraction peaks of PPy and MWCNTs are not found in cotton-PPy, cotton-PPy-MWCNTs and cotton-PPy-MWCNT-$BiVO_4$ composites. This is because that PPy is amorphous (Harraz et al. 2015) and the loading of MWCNTs on the fabric surface is less than 5% (Maity et al. 2018). After introducing $BiVO_4$ into the composite system, the strongest peak at $2\theta = 28.99°$ and secondary strong peak at $2\theta = 30.62°$ are found, corresponding to the (112) and (004) facet (Miao et al. 2016). No other impurity peaks were found in the XRD pattern, showing that only the monoclinic of $BiVO_4$ is introduced in the layered assembly process.

The chemical composition and chemical state of the cotton composite fabric are tested by XPS analyses. It can be clearly observed that C, N, O, Bi and V are the main elements in the composite fabric surface (Fig. 5a), which is consistent with the EDS analyses result. Figure 5b shows the high-resolution Bi 4f spectra consist of two peaks at 164.27 eV and 158.94 eV, which belong to Bi $4f_{5/2}$ and Bi $4f_{7/2}$, respectively. This proves that the Bi element in the composite fabric is in the Bi^{3+} ion state (Ou et al. 2018). The spectra in Fig. 5c demonstrates that C 1 s has two characteristic peaks, located in 289.5 eV and 284.5 eV. The former represents polypyrrole skeleton and sp^2 hybridized carbon (Liang et al. 2019), and the latter is mainly considered as C-O and hydroxy carbon (Jo and Sagaya Selvam 2016). The N 1 s spectra of composite fabric are shown in Fig. 5d,which is divided into two peaks at 405.77 eV and 399.63 eV, corresponding to C-N and N–H in Polypyrrole (Cai et al. 2017). The O 1 s spectra can be decomposed into

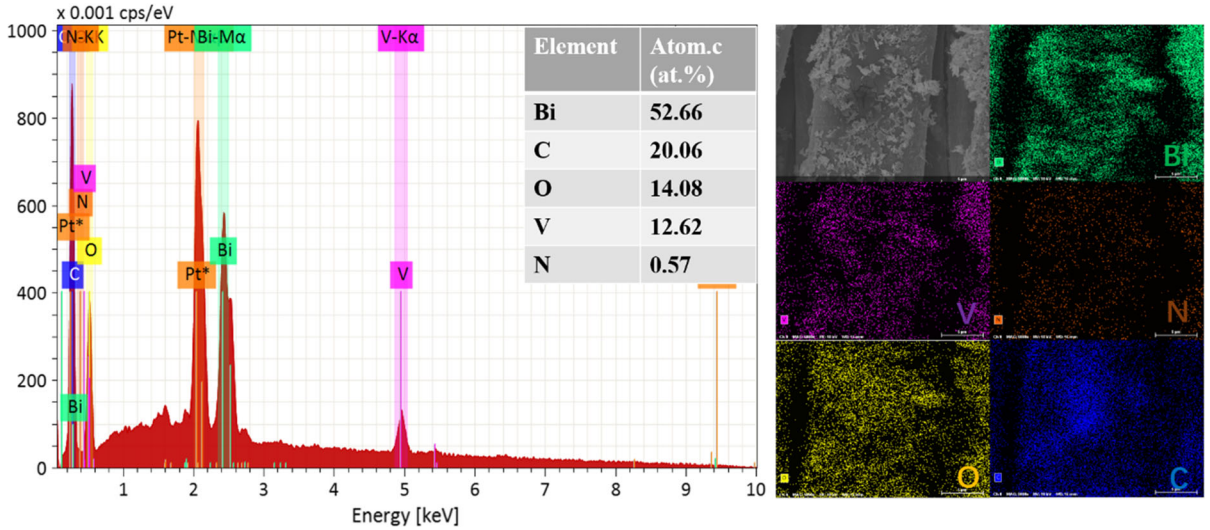

Fig. 3 EDS-mapping analysis of cotton-PPy-MWCNTs-$BiVO_4$ sample

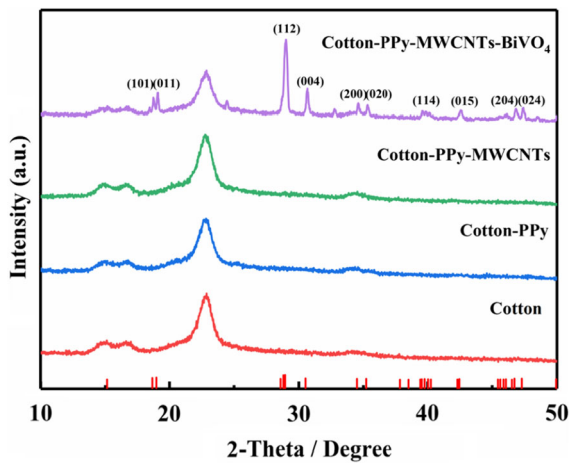

Fig. 4 XRD pattern of as-prepared samples

two adjacent peaks of 532.08 eV and 529.65 eV, representing O-C = O and lattice oxygen in $BiVO_4$ (Jo and Sagaya Selvam 2016; Ou et al. 2018), respectively. Figure 5f shows that V 2p spectrum has two peaks of 523.78 eV and 516.37 eV, which corresponds to the split of the V^{5+} spin orbit, indicating that V ions exhibit a valence of V^{+5} in the system (Wu et al. 2017a). The XPS analyses results demonstrate the chemical state of each element, which is consistent with the theoretical results of BiVO4, PPy and MWCNTs.

As shown in the Fig. 6a, UV–Vis diffuse reflection spectra (DRS) is used to study photo-selective absorption property of composite fabrics. Cotton-PPy-MWCNT-$BiVO_4$ possess better absorption properties than the three other control samples in the visible region of 400 ∼ 500 nm. The enhancement of visible light absorption is due to the introduction of monoclinic $BiVO_4$, which has higher photocatalytic activity. At the same time, cotton-PPy-MWCNTs also has a great level of light absorption considering the black color brought by MWCNTS. The improvement of cotton-PPy-MWCNTs in the full-band light absorption can further confirms this assumption. The enhancement of visible light absorption in cotton-PPy-MWCNT-$BiVO_4$ system is of great significance for improving photocatalytic performance. Furthermore, the band gap energy spectrum is obtained by the Kubelka–Munk equation (Sangiorgi et al. 2017) based on the UV–Vis diffuse reflectance data. As shown in Fig. 6b, the Eg of Cotton-PPy-MWCNT-$BiVO_4$ is approximately about 2.44 eV. Smaller band gap means the better carrier separation efficiency, which can increase the actual amount of active material and improve the efficiency of photocatalytic reaction.

Photocatalytic performance

Charges separation efficiency for the photocatalyst is characterized by PL spectra. As shown in Fig. 7a, the intensity of the peak at 426.9 nm gradually weakens with the component loaded on the cotton, which means that the recombination probability of

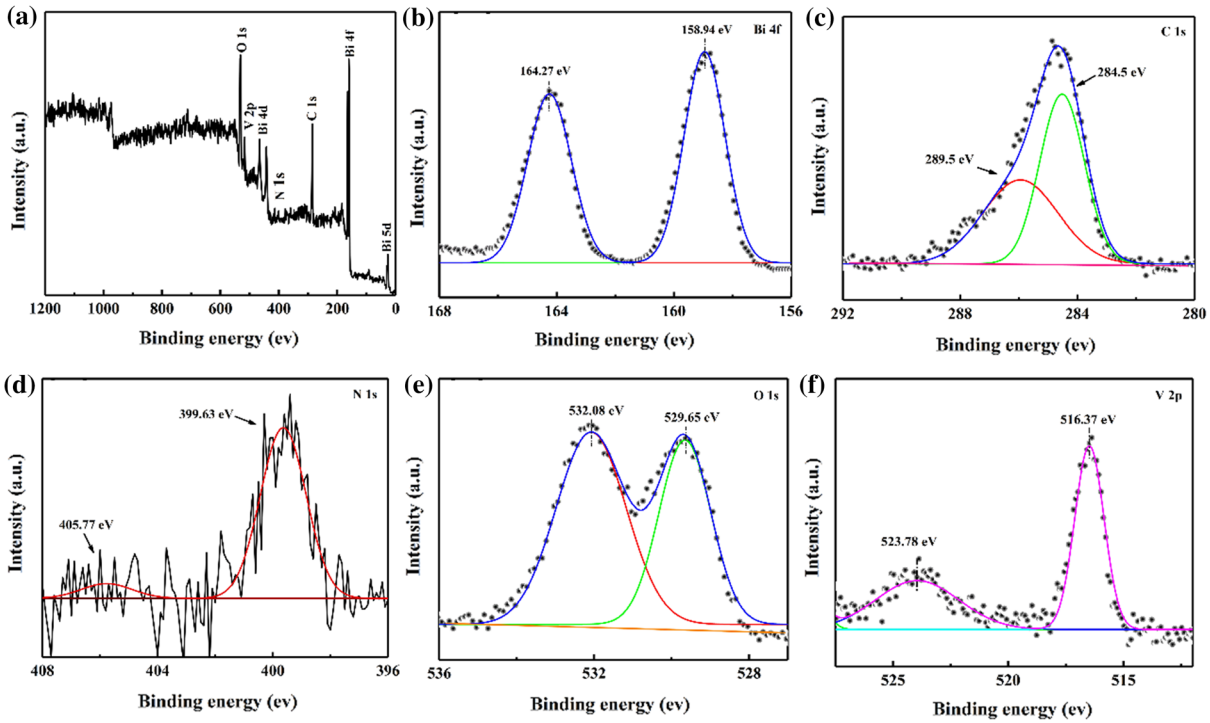

Fig. 5 **a** XPS survey spectra; high resolution XPS spectrum of **b** Bi 4f, **c** V 2p, **d** N 1 s, **e** C 1 s and **f** O 1 s

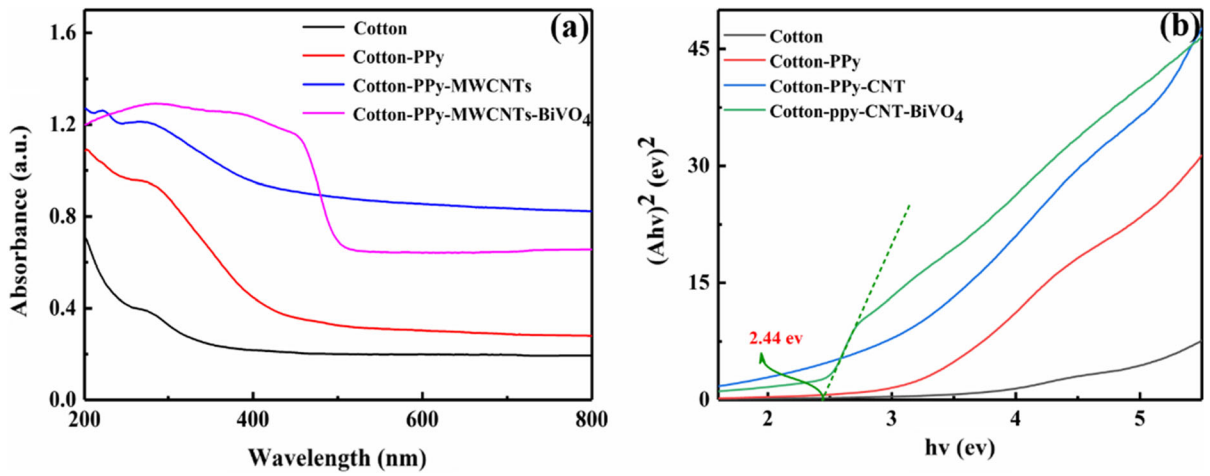

Fig. 6 **a** UV–Vis diffuse reflectance spectra of all the samples and **b** Band gap energy evaluation of all the samples

photogenerated charges and holes decrease with the loading of the components. Besides, this result reveals that PPy, MWCNTs and $BiVO_4$ tightly combine with each other and the combination can obviously improve the charges separation efficiency under visible light. The photocurrent response density is also a popular strategy to study charge separation efficiency, as shown in Fig. 7b. With the progress of radiation, it can be clearly visible that the photocurrent density of all four groups increases and the density increases with the superposition of the components. It indicates that the composite catalyst can generate electrons by light excitation and the separation efficiency of charges is improved especially after the introduction of $BiVO_4$.

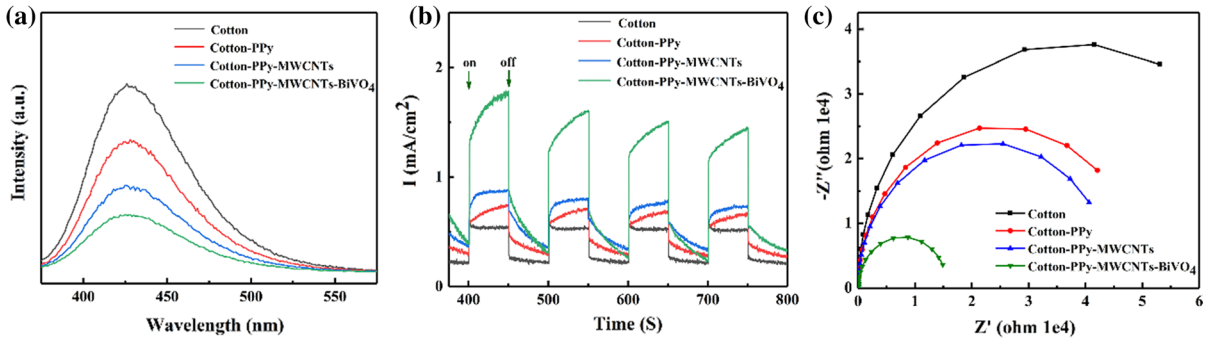

Fig. 7 **a** PL spectra for the different samples; **b** Photocurrent response and **c** EIS profiles

Therefore, the combination of PPy, MWCNTs and $BiVO_4$ plays a vital role in increasing the separation efficiency of charges.

Electrochemical impedance spectroscopy (EIS) is an efficient method to investigate the transfer and migration of charges, where the electron transfer rate is determined by the radius of the arc. As shown in Fig. 7c, the cotton fabric exhibits the largest arc radius, which indicates that it has a huge resistance. Subsequently, as the two conductive materials PPy and MWCNTs are loaded onto the cotton, the radius of the formed cotton-PPy and cotton-PPy-MWCNs system become smaller and the resistance gradually decreases. The further introduction of $BiVO_4$ dramatically reduces the radius of the arc, representing that the synergistic effect exists between $BiVO_4$, PPy and MWCNTs. The maximum separation of holes and electrons efficiency can only be achieved when $BiVO_4$, PPy and MWCNTs are in close contact. This synergistic effect greatly reduces the electric resistance and increases the electron transfer speed, thereby effectively reducing the probability of carrier recombination and improving photocatalytic activity.

The catalytic ability and absorption property of the prepared photocatalyst are evaluated by degrading RB-19. As shown in Fig. 8a, after incubation in the dark condition for 30 min, RB-19 is hardly absorbed by the cotton fabric, while the adsorption values for the cotton-PPy and cotton-PPy-MWCNTs are quite high. This phenomenon can be ascribed to the following reasons. Firstly, the reactive dye RB-19 is anionic and the pH of the dye solution is about 2.5. PPy will undergo protonation reaction under this pH condition, which can form bonds with the dye anion and increase the adsorption of the dye. Secondly, MWCNTs have good adsorption properties of dyes as they are a hollow tubular structure with a large specific surface area. After the introduction of $BiVO_4$, part of the originally exposed PPy and MWCNTs is covered. The adsorption capacity of the cotton-PPy-MWCNTs-$BiVO_4$ quaternary composite fabric is weakened, but remains at a high level. The strong adsorption capacity means that more dyes will be adsorbed on the surface of the catalyst, and the reaction opportunity of the dye with the active substances increases, thus improving the catalytic speed and efficiency (Hao et al. 2012; Yu et al. 2005). With the degradation of the adsorbed dye, the free dye in solution can almost be absorbed by the cotton composite fabric and the new degradation process is induced.

To better understand the degradation kinetics in the photocatalytic reaction, the apparent first-order model ($\ln C_0/C_t = K–t$) is used to fit the curve of the conversion against time. It is observed in Fig. 8b that all the photocatalytic processes fit well with the model and the slope of the line formed by the fit increases with the load of conductive components. The slope for the cotton-PPy-MWCNTs-$BiVO_4$ quaternary composite fabric is 2.9 times of that for the ternary system (cotton-PPy), which illustrates that the combination between PPy, MWCNTs and $BiVO_4$ can greatly accelerate the separation of photogenerated electrons and holes, thus greatly improving the degradation rate.

Stability and recyclability

In order to investigate the stability and reusability performance, the cycle experiment of the cotton-based composite photocatalytic materials is carried out. Degradation property and XRD test of the composite are shown in Fig. 9. The degradation efficiency of the RB-19 solution by cotton-PPy-MWCNTs-$BiVO_4$

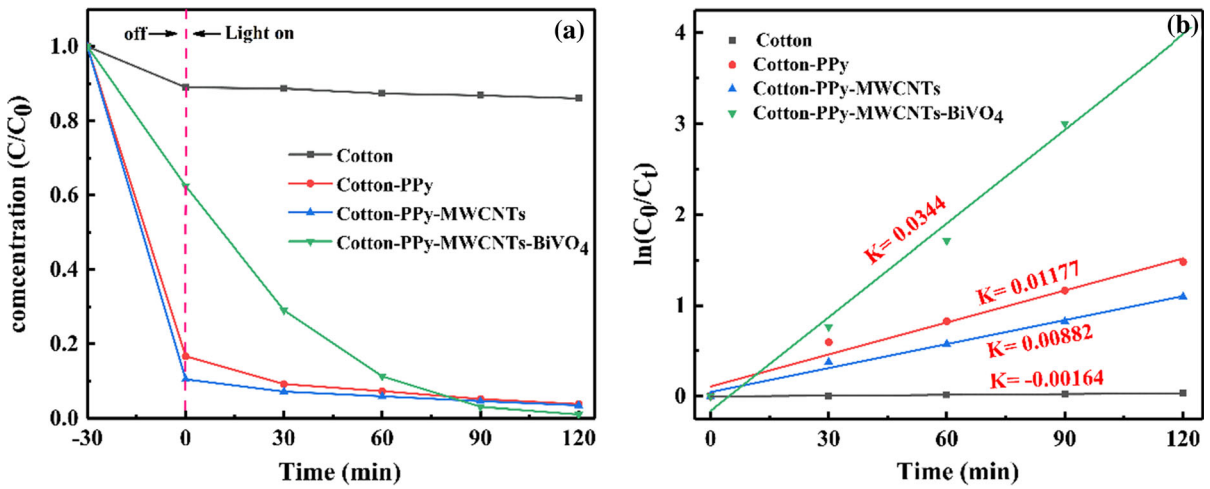

Fig. 8 **a** Photodegradation curves of RB-19; **b** Reaction kinetic curves of as-prepared samples corresponding to the photodegradation curves

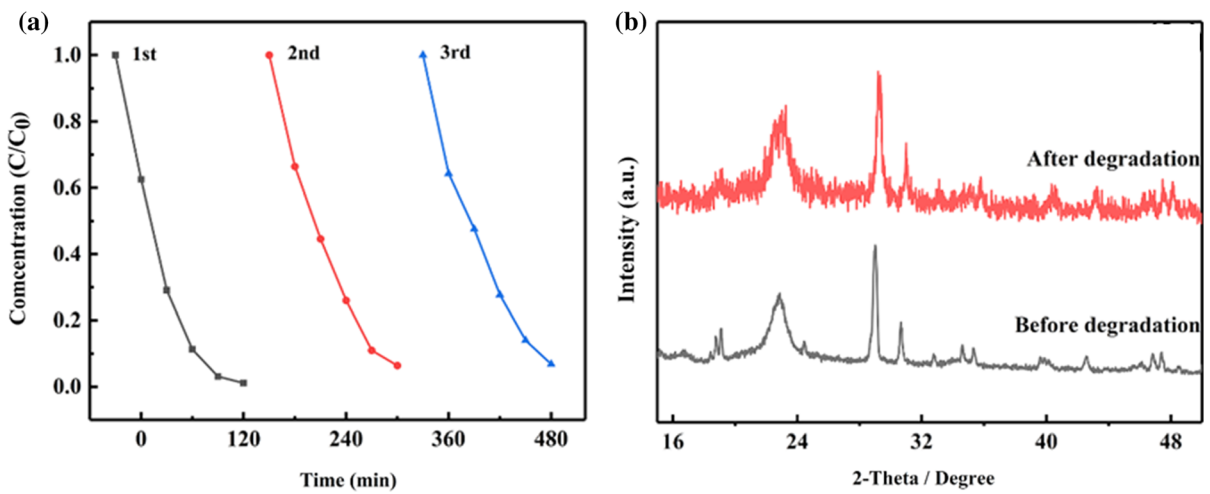

Fig. 9 **a** Cycling test for the photocatalytic degradation; **b** The XRD spectrum before degradation and after degradation

quaternary composite fabric within 2 h can still maintain at 90% after three cycles usage, indicating that this composite material has excellent cycling ability. The XRD spectrum of the composite cotton fabric sample after the degradation experiment do not show significant change compared with the unused sample, which further illustrates this catalyst is enough stable with reused. Therefore, the composite photocatalytic fabric not only has good degradation effect, but also maintains a high level of recyclability and stability.

Mechanism of degradation process

In the previous characterization, we demonstrate the successful preparation of composite photocatalytic materials and explore the degradation performance of pollutants by the catalyst. Why do composite photocatalytic materials have better degradation performance? To answer this question, the potential mechanism of the catalyst is explored. Firstly, the active material in the photocatalytic reaction is measured by a hole radical trapping experiment. Tert-butanol (t-BuOH), oxalate (Na-OA) and benzoquinone (BQ) are used as scavengers for hydroxyl

radicals, holes and superoxide ions, respectively and the result is shown in Fig. 10. Compared with the sample without the inhibitor, the degradation efficiency of the sample with t-BuOH do not change obviously, indicating that the hydroxyl radical is not the active substance of the reaction. In addition, the degradation efficiency of the samples is reduced after adding Na-OA and BQ. Especially after adding Na-OA for 2 h, the efficiency is only about 28% of that without capture agent, illustrating that the active substances in the catalytic reaction are mainly holes and partial superoxide ion.

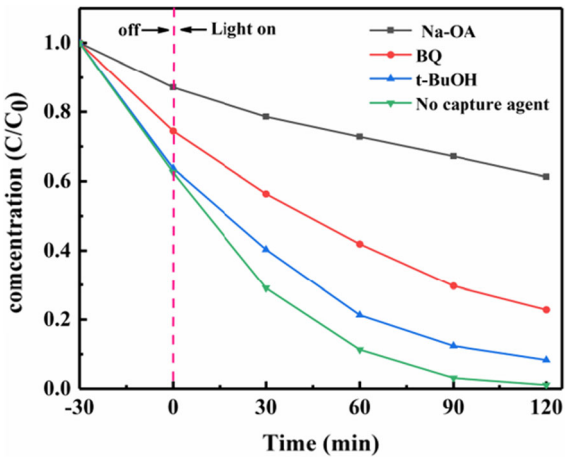

Fig. 10 Photodegradation curves of RB-19 over cotton-PPy-MWCNTs-$BiVO_4$ composite with different active species scavengers under visible light irradiation

According to the above analysis results, the possible photocatalytic mechanism of composite cotton fabric is proposed as shown in Fig. 11. Firstly, when the incident photon energy is greater than or equal to the band gap of $BiVO_4$, electrons on the valence band are excited to the conduction band and leave positively charged holes on the valence band. However, if no other substances are added to the system, the electrons will quickly return to the valence band and recombine with the holes due to the instability of the excited state. According to the previous DRS analysis results, the band gap of $BiVO_4$ is 2.44 eV, where the conduction band positions and the valence band positions are + 0.34 eV and + 2.78 eV (Bao et al. 2016), respectively. PPy has a higher LUMO potentials (− 1.15 eV) and HOMO potentials (+ 1.05 eV) than that of $BiVO_4$ (Li et al. 2017). When PPy is introduced into the system, the excited photogenerated electron holes will transfer to PPy firstly, and the electrons on PPy will aggregate on the conduction band of $BiVO_4$. In addition, the photogenerated electrons accumulated on the conduction band can be transferred to the surface through a well-conducting carbon tube because of the tight contact between $BiVO_4$ and MWCNTs, and then form superoxide ions with oxygen. In this way, the separation of holes and electrons is achieved, and the generated holes and

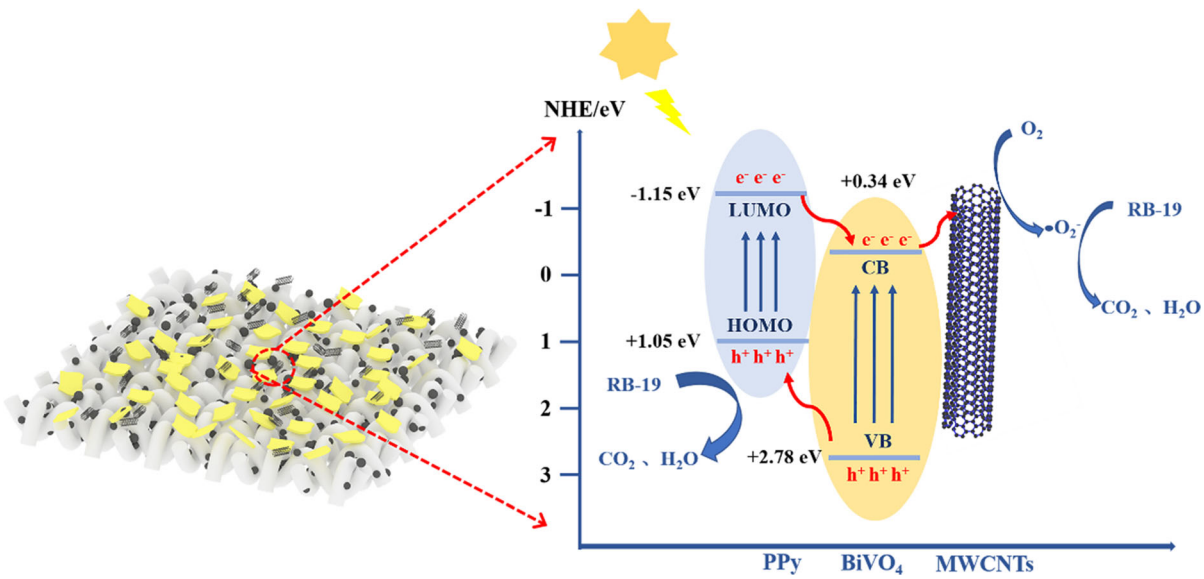

Fig. 11 The possible photocatalytic reaction mechanism of PPy-MWCNTs-$BiVO_4$ for degradation under visible-light irradiation

superoxide ions mineralize the dyes adsorbed on the surface, thereby degrading organic contaminants. Meanwhile, the large specific surface area of MWCNTs and the protonation reaction of PPy under acidic conditions greatly enhance the adsorption capacity of the composite fabric, and more reaction sites are generated. Hence, the reaction equations involved in the catalytic process are shown as follows:

$$\mathrm{PPy/MWCNTs}/BiVO_4 + \mathrm{hv} \rightarrow e^- + h^+$$

$$e^- + O^2 \rightarrow O_2^-$$

$$O_2^- + h^+ + \mathrm{RB} - 19 \rightarrow CO_2 + H_2O$$

Conclusion

In summary, a novel cotton-PPy-MWCNTs-$BiVO_4$ composite photocatalytic system was successfully prepared by a simple layer assembly method. With the introduction of PPy, MWCNTs and $BiVO_4$ components, the composite system shows excellent catalytic activity and can completely degrade RB-19 dye solution within two hours. The improvement of catalytic degradation ability stems from the coupling between PPy, MWCNTs and $BiVO_4$. PPy and MWCNTs can efficiently transfer holes and separate electrons respectively, which greatly improves the separation efficiency. In addition, the composite photocatalytic cotton fabric material exhibits good cycle stability, and the degradation performance after three cycles can still be maintained at 90%. This research provides a broad perspective for the application of cellulose-based multilayer flexible photocatalytic materials in the wastewater treatment.

Acknowledgments This work was financially funding by the Supported by the Fundamental Research Funds for the Central Universities (Grant No. 2232020G-01) and Guangxi Innovation Drive Development Fund (Grant No. AA17204076) and Zhejiang Province Public Welfare Technology Application Research Project (CN) (Grant No. LGG18E030002).

References

Malathi A, Madhavan J, Ashokkumar M, Arunachalam P (2018) A review on BiVO 4 photocatalyst: activity enhancement methods for solar photocatalytic applications. Appl Catal A General 555:47–74. https://doi.org/10.1016/j.apcata.2018.02.010

Bao N, Yin Z, Zhang Q, He S, Hu X, Miao X (2016) Synthesis of flower-like monoclinic BiVO 4 /surface rough TiO 2 ceramic fiber with heterostructures and its photocatalytic property. Ceram Int 42:1791–1800. https://doi.org/10.1016/j.ceramint.2015.09.142

Cai L, Jiang H, Wang L (2017) Enhanced photo-stability and photocatalytic activity of Ag3PO4 via modification with BiPO4 and polypyrrole. Appl Surf Sci 420:43–52. https://doi.org/10.1016/j.apsusc.2017.05.135

Crake A et al (2019) Titanium dioxide/carbon nitride nanosheet nanocomposites for gas phase CO2 photoreduction under UV-visible irradiation. Appl Catal B Environ 242:369–378. https://doi.org/10.1016/j.apcatb.2018.10.023

Dai W, Yu J, Deng Y, Hu X, Wang T, Luo X (2017) Facile synthesis of MoS2/Bi2WO6 nanocomposites for enhanced CO2 photoreduction activity under visible light irradiation. Appl Surf Sci 403:230–239. https://doi.org/10.1016/j.apsusc.2017.01.171

Dong X et al (2019) Monodispersed CuFe2O4 nanoparticles anchored on natural kaolinite as highly efficient peroxymonosulfate catalyst for bisphenol A degradation. Appl Catal B Environ 253:206–217. https://doi.org/10.1016/j.apcatb.2019.04.052

Fan J, Yu D, Wang W, Liu B (2019) The self-assembly and formation mechanism of regenerated cellulose films for photocatalytic degradation of C.I. Reactive Blue 19. Cellulose 26:3955–3972. https://doi.org/10.1007/s10570-019-02350-y

Han H, Fu M, Li Y, Guan W, Lu P, Hu X (2018) In-situ polymerization for PPy/g-C 3 N 4 composites with enhanced visible light photocatalytic performance. Chinese J Catal 39:831–840. https://doi.org/10.1016/s1872-2067(17)62997-8

Hao R, Xiao X, Zuo X, Nan J, Zhang W (2012) Efficient adsorption and visible-light photocatalytic degradation of tetracycline hydrochloride using mesoporous BiOI microspheres. J Hazard Mater 209–210:137–145. https://doi.org/10.1016/j.jhazmat.2012.01.006

Harraz FA, Ismail AA, Al-Sayari SA, Al-Hajry A (2015) Novel α-Fe2O3/polypyrrole nanocomposite with enhanced photocatalytic performance. J Photochem Photobiol A Chem 299:18–24. https://doi.org/10.1016/j.jphotochem.2014.11.001

Jo W-K, Sagaya Selvam NC (2016) Fabrication of photostable ternary CdS/MoS 2 /MWCNTs hybrid photocatalysts with enhanced H 2 generation activity. Appl Catal A General 525:9–22. https://doi.org/10.1016/j.apcata.2016.06.036

Komeily-Nia Z, Montazer M, Heidarian P, Nasri-Nasrabadi B (2019) Smart photoactive soft materials for environmental cleaning and energy production through incorporation of nanophotocatalyst on polymers and textiles. Polym Adv Technol 30:235–253. https://doi.org/10.1002/pat.4480

Kyzas GZ, Matis KA (2015) Nanoadsorbents for pollutants removal: a review. J Mol Liq 203:159–168. https://doi.org/10.1016/j.molliq.2015.01.004

Legrini O, Oliveros E, Braun AM (1993) Photochemical processes for water treatment. Chem Rev 93:671–698. https://doi.org/10.1021/cr00018a003

Li M, Liu F, Ma Z, Liu W, Liang J, Tong M (2019) Different mechanisms for E. coli disinfection and BPA degradation by CeO2-AgI under visible light irradiation. Chem Eng J 371:750–758. https://doi.org/10.1016/j.cej.2019.04.036

Li X et al (2017) Precisely locate Pd-Polypyrrole on TiO 2 for enhanced hydrogen production. Int J Hydrog Energy 42:25195–25202. https://doi.org/10.1016/j.ijhydene.2017.08.153

Liang Y, Wang X, An W, Li Y, Hu J, Cui W (2019) A g-C3N4@ppy-rGO 3D structure hydrogel for efficient photocatalysis. Appl Surf Sci 466:666–672. https://doi.org/10.1016/j.apsusc.2018.10.059

Lin L, Yu D, Wang W, Gao P, Bu K, Liu B (2016) Preparation of BiVO4/Bi2WO6/multi-walled carbon nanotube nanocomposites for enchaning photocatalytic performance. Mater Lett 185:507–510. https://doi.org/10.1016/j.matlet.2016.09.063

Liu X, Cai L (2018) Novel indirect Z-scheme photocatalyst of Ag nanoparticles and polymer polypyrrole co-modified BiOBr for photocatalytic decomposition of organic pollutants. Appl Surf Sci 445:242–254. https://doi.org/10.1016/j.apsusc.2018.03.178

Liu Y et al (2019) Facet effect on the photoelectrochemical performance of a WO3/BiVO4 heterojunction photoanode. Appl Catal B Environ 245:227–239. https://doi.org/10.1016/j.apcatb.2018.12.058

Lv C, Chen G, Sun J, Zhou Y, Fan S, Zhang C (2015) Realizing nanosized interfacial contact via constructing BiVO 4 /Bi 4 V 2 O 11 element-copied heterojunction nanofibres for superior photocatalytic properties. Appl Catal B Environ 179:54–60. https://doi.org/10.1016/j.apcatb.2015.05.022

Lv N, Li Y, Huang Z, Li T, Ye S, Dionysiou DD, Song X (2019) Synthesis of GO/TiO2/Bi2WO6 nanocomposites with enhanced visible light photocatalytic degradation of ethylene. Appl Catal B Environ 246:303–311. https://doi.org/10.1016/j.apcatb.2019.01.068

Ma J, Huang D, Zou J, Li L, Kong Y, Komarneni S (2014) Adsorption of methylene blue and Orange II pollutants on activated carbon prepared from banana peel. J Porous Mater 22:301–311. https://doi.org/10.1007/s10934-014-9896-2

Maity D, Rajavel K, Kumar RTR (2018) Polyvinyl alcohol wrapped multiwall carbon nanotube (MWCNTs) network on fabrics for wearable room temperature ethanol sensor. Sens Actuators B Chem 261:297–306. https://doi.org/10.1016/j.snb.2018.01.152

Miao G, Huang D, Ren X, Li X, Li Z, Xiao J (2016) Visible-light induced photocatalytic oxidative desulfurization using BiVO 4 /C 3 N 4 @SiO 2 with air/cumene hydroperoxide under ambient conditions. Appl Catal B Environ 192:72–79. https://doi.org/10.1016/j.apcatb.2016.03.033

Ou M et al (2018) Hierarchical Z-scheme photocatalyst of g-C3N4@Ag/BiVO4 (040) with enhanced visible-light-induced photocatalytic oxidation performance. Appl Catal B Environ 221:97–107. https://doi.org/10.1016/j.apcatb.2017.09.005

Ran J, Zhu B, Qiao SZ (2017) Phosphorene Co-catalyst Advancing Highly Efficient Visible-Light Photocatalytic Hydrogen Production. Angew Chem Int Ed Engl 56:10373–10377. https://doi.org/10.1002/anie.201703827

Safaei J et al (2018) Enhanced photoelectrochemical performance of Z-scheme g-C3N4/BiVO4 photocatalyst. Appl Catal B Environ 234:296–310. https://doi.org/10.1016/j.apcatb.2018.04.056

Sangiorgi N, Aversa L, Tatti R, Verucchi R, Sanson A (2017) Spectrophotometric method for optical band gap and electronic transitions determination of semiconductor materials. Opt Mater 64:18–25. https://doi.org/10.1016/j.optmat.2016.11.014

Tasbihi M, Fresno F, Simon U, Villar-García IJ, Pérez-Dieste V, Escudero C, de la Peña O'Shea VA (2018) On the selectivity of CO2 photoreduction towards CH4 using Pt/TiO2 catalysts supported on mesoporous silica. Appl Catal B Environ 239:68–76. https://doi.org/10.1016/j.apcatb.2018.08.003

Trowbridge A, Reich D, Gaunt MJ (2018) Multicomponent synthesis of tertiary alkylamines by photocatalytic olefin-hydroaminoalkylation. Nature 561:522–527. https://doi.org/10.1038/s41586-018-0537-9

Wacławek S, Lutze HV, Grübel K, Padil VVT, Černík M, Dionysiou DD (2017) Chemistry of persulfates in water and wastewater treatment: a review. Chem Eng J 330:44–62. https://doi.org/10.1016/j.cej.2017.07.132

Wang J et al (2019) Photocatalytic hydrogen evolution on P-type tetragonal zircon BiVO4. Appl Catal B Environ 251:94–101. https://doi.org/10.1016/j.apcatb.2019.03.049

Wang Y, Ding K, Xu R, Yu D, Wang W, Gao P, Liu B (2020) Fabrication of BiVO4/BiPO4/GO composite photocatalytic material for the visible light-driven degradation. J Clean Produc. https://doi.org/10.1016/j.jclepro.2019.119108

Wang Y et al (2018) Photocatalytic properties of the g-C3N4/{010} facets BiVO4 interface Z-Scheme photocatalysts induced by BiVO4 surface heterojunction. Appl Catal B Environ 234:37–49. https://doi.org/10.1016/j.apcatb.2018.04.026

Wu X et al (2017a) Carbon dots as solid-state electron mediator for BiVO4/CDs/CdS Z-scheme photocatalyst working under visible light. Appl Catal B Environ 206:501–509. https://doi.org/10.1016/j.apcatb.2017.01.049

Wu Z et al (2017b) Electrically Insulated Epoxy Nanocomposites Reinforced with Synergistic Core-Shell SiO2 MWCNTs and Montmorillonite Bifillers. Macromole Chem Phys. https://doi.org/10.1002/macp.201700357

Xiao M et al (2018) Hollow nanostructures for photocatalysis: advantages and challenges. Adv Mater. https://doi.org/10.1002/adma.201801369

Xu T, Wang D, Dong L, Shen H, Lu W, Chen W (2019) Graphitic carbon nitride co-modified by zinc phthalocyanine and graphene quantum dots for the efficient photocatalytic degradation of refractory contaminants. Appl Catal B 244:96–106. https://doi.org/10.1016/j.apcatb.2018.11.049

Yang R, Dong F, You X, Liu M, Zhong S, Zhang L, Liu B (2019) Facile synthesis and characterization of interface charge transfer heterojunction of Bi2MoO6 modified by Ag/AgCl photosensitive material with enhanced photocatalytic activity. Mater Lett 252:272–276. https://doi.org/10.1016/j.matlet.2019.06.006

Yang R, Zhu Z, Hu C, Zhong S, Zhang L, Liu B, Wang W (2020) One-step preparation (3D/2D/2D) BiVO4/FeVO4@rGO heterojunction composite photocatalyst for the removal of tetracycline and hexavalent chromium ions in water. Chem Eng J. https://doi.org/10.1016/j.cej.2020.124522

Yu Y et al (2005) Enhancement of adsorption and photocatalytic activity of TiO2 by using carbon nanotubes for the treatment of azo dye. Appl Catal B Environ 61:1–11. https://doi.org/10.1016/j.apcatb.2005.03.008

Zhang G, Lan ZA, Wang X (2016) Conjugated polymers: catalysts for photocatalytic hydrogen evolution. Angew Chem Int Ed Engl 55:15712–15727. https://doi.org/10.1002/anie.201607375

Zhao D et al (2017) One-step synthesis of composite material MWCNT@BiVO4 and its photocatalytic activity. RSC Adv 7:33671–33679. https://doi.org/10.1039/c7ra04288d

Zhou H, Wen Z, Liu J, Ke J, Duan X, Wang S (2019) Z-scheme plasmonic Ag decorated WO3/Bi2WO6 hybrids for enhanced photocatalytic abatement of chlorinated-VOCs under solar light irradiation. Appl Catal B Environ 242:76–84. https://doi.org/10.1016/j.apcatb.2018.09.090